

Demographic stochasticity and resource autocorrelation control biological invasions in heterogeneous landscapes

Andrea Giometto^{1,2,*}

Florian Altermatt^{2,3,*}

Andrea Rinaldo^{1,4}

1. Laboratory of Ecohydrology, School of Architecture, Civil and Environmental Engineering, École Polytechnique Fédérale de Lausanne, CH-1015 Lausanne, Switzerland;
2. Eawag, Swiss Federal Institute of Aquatic Science and Technology, Department of Aquatic Ecology, CH-8600 Dübendorf, Switzerland;
3. Department of Evolutionary Biology and Environmental Studies, University of Zürich, CH-8057 Zürich, Switzerland;
4. Dipartimento di Ingegneria Civile, Edile ed Ambientale, Università di Padova, I-35131 Padua, Italy.

* Corresponding author; e-mail: andrea.giometto@epfl.ch and florian.altermatt@eawag.ch.

Keywords: Environmental stochasticity, Biological invasions, Traveling waves, Front propagation, Fisher-Kolmogorov, Dispersal.

Abstract

Classical models of biological invasions assess species spread in homogeneous landscapes by assuming constant growth rates and random local movement. Mounting evidence suggests, however, that demographic stochasticity, environmental heterogeneity and non-random movement of individuals affect considerably the spread dynamics. Here, we show that the dynamics of biological invasions are controlled by the spatial heterogeneity of the resource distribution. We show theoretically that increasing the landscape resource autocorrelation length causes a reduction in the average speed of species spread. Demographic stochasticity plays a key role in the slowdown, which is strengthened when individuals can actively move towards resources. The reduction in the front propagation speed is verified in laboratory microcosm experiments with the flagellated protist *Euglena gracilis* by comparing spread in habitats characterized by different resource heterogeneity. Our theoretical and experimental findings highlight the need to account for the intrinsic stochasticity of population dynamics to describe spread in spatially extended landscapes, which are inevitably characterized by heterogeneous spatial distributions of resources controlling vital rates. Our work identifies the resource autocorrelation length as a key modulator and a simple measure of landscape susceptibility to biological invasions, with implications for predicting the characters of biological invasions within naturally heterogeneous environmental corridors.

Introduction

Environmental fluctuations and heterogeneity are ubiquitous in nature and are thought to affect nearly all aspects of ecology, ranging from species coexistence to population synchrony, driving range shifts and potentially causing abrupt biotic change (e.g., Nelson 2012; With 2002; With and Crist 1995). Local population dynamics in fluctuating and heterogeneous environments have been studied extensively in recent years (Duncan et al. 2013; Gonzalez and Holt 2002), mainly with respect to population synchrony (Benton et al. 2001; Fox et al. 2011; Vasseur and Fox 2009). Both theoretical (Roy et al. 2005; Vasseur 2007) and experimental (Fontaine and Gonzalez 2005; Gonzalez and Holt 2002; Massie et al. 2015) studies have highlighted the relevance of the temporal autocorrelation structure of environmental fluctuations for ecological dynamics. The study of ecological processes in the presence of environmental stochasticity at different levels of autocorrelation is of interest not only because environmental fluctuations are typically positively correlated (Benincà et al. 2011), but also in view of the global shift towards ‘bluer’ climate variables (i.e., more fluctuating) across most continents (e.g., García-Carreras and Reuman 2011). Whereas most experimental investigations focused on temporal environmental fluctuations, spatial heterogeneity received surprisingly little attention (Melbourne et al. 2007; With 2002). Accordingly, the study of the implications of environmental fluctuations for spatial dynamics (Duncan et al. 2013; Gonzalez and Holt 2002) and especially for the propagation of biological invasions (Méndez et al. 2011; Neubert et al. 2000; With 2002) is a challenging avenue for experimental research.

The effect of environmental fluctuations and spatial heterogeneity may be especially relevant in the context of biological invasions and range shifts, which are seen as some of the most relevant current dynamics across all ecosystems (Hastings et al. 2005). The spatial spread of invasions has been investigated extensively in the literature, starting with the pioneering works of Fisher, Kolmogorov and Skellam (Fisher 1937; Kolmogorov et al. 1937; Skellam 1951). Traditionally, the propagation of invasive fronts has been modeled with the Fisher-Kolmogorov equation (Fisher 1937; Kolmogorov et al. 1937) that predicts a linear rate of spread in homogeneous environments. Such equation was applied extensively to describe field data (Andow et al. 1990; Lubina and Levin 1988) and found applications also in other disciplines, for example physics and chemistry (Méndez et al. 2010). Comprehensive reviews of mathematical modeling and empirical studies of species spread exist (Hastings et al. 2005). Stochastic generalizations of the Fisher-Kolmogorov equation showed that demographic stochasticity affects the propagation dynamics, causing a reduction in the front propagation speed (Hallatschek and Korolev 2009). Other modeling approaches have shown that temporal fluctuations in mean dispersal distances can increase invasion speed, while temporally uncorrelated fluctuations in demographic parameters typically decrease the front propagation velocity (Ellner and Schreiber 2012; Méndez et al. 2011). Despite the fact that most natural environments are inevitably heterogeneous (e.g., Holyoak et al. 2005), however, much of the current understanding of species spread is based on theoretical models (Hastings et al. 2005; Méndez et al. 2010) that considered homogeneous landscapes. Only in recent years, progress has been achieved in the theoretical understanding of species spread in more complex, heterogeneous or fluctuating landscapes (Dewhurst and Lutscher 2009; Melbourne et al. 2007; Méndez et al. 2010; Nelson and Schnerb 1998; Neubert et al. 2000; Pachepsky and Levine 2011), and such progress calls for experimental verification (Seymour and Altermatt 2014). For example, thresholds for the minimal percentage of favorable habitat that can support spread have been studied (Dewhurst and Lutscher 2009; With 2002; With and Crist 1995). Dewhurst and Lutscher (2009), for example, derived quantitative relationships for the invasion threshold and spread

rates in integro-differential equation models in fragmented landscapes. The speed of biological invasions has been claimed to be affected by environmental stochasticity (Méndez et al. 2011) and an extensive line of research addressed the contribution of geometrical heterogeneities of the landscape to the propagation of invading fronts (Bertuzzo et al. 2007; Campos et al. 2006; Méndez et al. 2004; Méndez et al. 2003; Seymour and Altermatt 2014) suggesting that, in general, geometrical heterogeneities slow the speed of front propagation.

Integrating environmental heterogeneity in models of spread is a challenging task and a modeling framework that allows drawing general conclusions is lacking to date (Hastings et al. 2005; Urban et al. 2008). In the search for such a framework, the study of biological invasions in heterogeneous and fluctuating environments has been addressed in the context of the Fisher-Kolmogorov equation (Fisher 1937; Kolmogorov et al. 1937) either by embedding various sources of environmental stochasticity in the original deterministic equation (Méndez et al. 2003, 2011; Shigesada et al. 1986) or by considering spread in spatially heterogeneous media (Bertuzzo et al. 2007; Campos et al. 2006; Méndez et al. 2004; Méndez et al. 2003). Environmental stochasticity and spatial heterogeneity (Nelson 2012; Nelson and Schnerb 1998) have been incorporated in the Fisher-Kolmogorov equation through noise terms that were uncorrelated in space, periodic in space (Kinezaki et al. 2003; Shigesada et al. 1986) or else characterized by a gaussian spatial correlation function with a fixed correlation length (Méndez et al. 2011). Whereas the importance of the autocorrelation structure of temporal environmental fluctuations for local ecological processes is now widely recognized (Fontaine and Gonzalez 2005; García-Carreras and Reuman 2011; Gonzalez and Holt 2002; Vasseur 2007), the effect of the spatial autocorrelation of environmental fluctuations on biological spread rates has just begun to be explored (Urban et al. 2008). The experimental study of species spread has recently started to test theoretical predictions of the Fisher-Kolmogorov model in homogeneous habitats (Croze et al. 2011; Giometto et al. 2014; Korolev et al. 2011; Simpson et al. 2013). A limited number of empirical works has measured spread rates in heterogeneous and diverse habitats and compared realized spread distances in patchily distributed sites (Bailey et al. 2000; Bergelson et al. 1994; Williamson and Harrison 2002). However, the results of these studies were not linked to Fisher-Kolmogorov-like models embedding environmental stochasticity or heterogeneity. In particular, experimental studies investigating the role of the resource autocorrelation structure in driving the spread of species are lacking.

Here, we study biological invasions in the presence of spatially heterogeneous resource distributions, which could, for example, reflect the spatial composition and quality of soil or topographically determined habitat elements such as exposure or elevation, or habitat fragmentation due to human land-use (e.g., With 2002; With and Crist 1995). Motivated by previous research on environmental fluctuations mentioned above, we focus on the effect of the spatial autocorrelation structure of the resource distribution on the propagation speed of biological invasion fronts. The distribution of resources is assumed to affect both the growth dynamics and movement behavior of individuals. Giometto et al. (2014) showed that, in homogeneous landscapes, demographic stochasticity introduces a noise term in the reaction-diffusion equation describing the front propagation, leading to a quantifiable variability of the process across replicated experimental invasions. Therefore, our tenet is that both environmental and demographic stochasticity jointly affect biological invasions and thus the interplay between these two sources of stochasticity is specifically investigated here.

We first show theoretically that the speed of species spread decreases when the resource autocorrelation length increases, all other conditions being equal. Second, we verify such prediction in a microcosm experiment with the flagellated protist *Euglena gracilis*, by manipulating light intensity profiles along lin-

ear landscapes (light is an energy source for *E. gracilis*, as it has chloroplasts and can photosynthesize). Third, we discuss the contribution of each process included in the model to the propagation of biological invasions. We show theoretically that demographic stochasticity is necessary to produce the slowdown, which is more pronounced if individuals can direct their movement towards resources.

Methods

Model

Species spread in heterogeneous linear landscapes is modeled via a stochastic generalization of the Fisher-Kolmogorov equation including demographic stochasticity (Bonachela et al. 2012; Dornic et al. 2005; Giometto et al. 2014):

$$\frac{\partial \rho}{\partial t} = D \frac{\partial^2 \rho}{\partial x^2} + r(I)\rho \left[1 - \frac{\rho}{K}\right] + \sigma \sqrt{\rho} \eta, \quad (1)$$

where $\rho(x, t)$ is the density of individuals, D is the diffusion coefficient of the species driven by the active movement of individuals, r is the growth rate, K is the carrying capacity, σ is a parameter describing the amplitude of demographic stochasticity and η is a gaussian, zero-mean white noise (i.e., the noise has correlations $\langle \eta(x, t) \eta(x', t') \rangle = \delta(x - x') \delta(t - t')$, where δ is the Dirac's delta function). Itô's stochastic calculus is adopted, as appropriate for the demographic noise term (Giometto et al. 2014). The growth rate $r(I) = r_0 I$ is assumed to be a function of the local amount of resources $I(x)$, which can assume two values: $I(x) = 1$ or $I(x) = 0$. Landscape heterogeneity is thus embedded in the resource profile $I(x)$. We studied the dimensionless form of equation (1), which reads (see app. A available online):

$$\frac{\partial \rho'}{\partial t'} = \frac{\partial^2 \rho'}{\partial x'^2} + \chi_I \rho' [1 - \rho'] + \sigma'' \sqrt{\rho'} \eta, \quad (2)$$

where $t' = r_0 t$, $x' = \sqrt{\frac{D}{r_0}} x$, $\rho' = \rho / K$, $\sigma'' = \frac{\sigma}{\sqrt{K(rD)^{1/4}}}$ and $\chi_I(x')$ is the indicator function of the set of x' for which $I(x') = 1$. In the following we drop primes for convenience: one can recover the original dimensions by multiplying t by r_0 , x by $\sqrt{r_0 D}$ and rescaling ρ and σ as indicated above. Numerical integration of stochastic partial differential equations with square root noise terms require ad hoc numerical methods, as standard approaches such as the first-order explicit Euler method inevitably produce unphysical negative values for the density ρ (Dornic et al. 2005). Therefore, equation (2) was integrated with the split-step method proposed in Dornic et al. (2005), see app. A for details.

We generated landscapes with various resource autocorrelation lengths by imposing $I(x)$ to be composed of subsequent independent patches of suitable ($I(x) = 1$ and $r = r_0$) or unsuitable ($I(x) = 0$ and $r = 0$) habitats (fig. 1A). The length of each patch was drawn from an exponential distribution with rate μ . Therefore, each landscape was a stochastic realization of the so-called telegraph process with rate μ and autocorrelation length $c_L = 1/(2\mu)$. The mean extent of suitable and unsuitable patches in such landscapes is $1/\mu$. Because simulated landscapes were finite, we only accepted landscapes with mean resources equal to $\bar{I} = L^{-1} \int_0^L I(x) dx = 1/2$ and autocorrelation length confined to a narrow window around $1/(2\mu)$. Examples of landscapes used in the simulations are shown in fig. 1A.

We generated 96 landscapes for each value of resource autocorrelation length c_L and integrated equation (2) numerically for each landscape and for each value of $\sigma \in \{0.1, 0.2, 0.4, 0.6\}$ (fig. 1B), with initial density profiles localized at the origin. To avoid the extinction of the whole population, we fixed the left

boundary at $\rho = 1$. For each numerical integration, we measured the position of the front by fixing a threshold value of the density ($\bar{\rho} = 0.15$) and recording the furthest point from the origin where the cell density was higher than such value. The mean propagation speed for each value of the resource autocorrelation length was computed by fitting a straight line (least-squares fit) to the mean front position versus time in the asymptotic propagation regime (fig. A6), before any of the replicated invasions reached the end of the landscape.

We derived a theoretical approximation to the mean front propagation speed, valid for large autocorrelation lengths c_L and σ , by characterizing the mean time taken to cross a patch of unfavorable habitat (where $I = r = 0$) of length z . Such mean time is shown (app. A) to depend on z and σ as $\langle \tau \rangle(z, \sigma) = Cz^2 e^{d(z\sigma^b)^a}$, where C , a , b and d are constants, independent of z and σ . Additionally, we characterized the functional dependence of the variance of τ on z and σ and derived an approximation to the variance of the total time taken by a front to colonize completely a landscape of finite length L (app. A). Our approximation is in good agreement with numerical integrations of equation (2) (fig. A4).

To test whether deterministic models predict a slowdown of the invading front for increasing resource autocorrelation length, we numerically integrated equation (2) with $\sigma = 0$. Additionally, we numerically integrated equation (2) with $\sigma = 0$ and imposing a negative growth rate r in unfavorable patches where $I = 0$ (app. A).

Experiments

We performed experiments with the flagellated protist *Euglena gracilis*, acquired from Carolina Biological Supply (NC, USA). A culture of *E. gracilis* was initialized two weeks prior to the start of the experiment and kept at 22 °C under constant LED (Light Emitting Diode, model SMD 5050) light of wavelength 469 nm (emission width approximately 10 nm), in a filtered (0.2 μm filter) nutrient medium composed of sterilized spring water and Protozoan Pellets (Carolina Biological Supply, NC, USA) at a density of 0.45 $\text{g}\cdot\text{l}^{-1}$ in a 500 ml Schott flask (Altermatt et al. 2015).

In our experiment, light was used as the energy source for *E. gracilis*. To demonstrate that light was crucial for the growth of *E. gracilis* in our experimental setting, we measured *E. gracilis*' growth curves (fig. 4A) by initializing eight low-density cultures in 10 ml cell culture flasks. Half of such cultures were placed on top of two LEDs (for each culture) operated at a total flux of 1 mW each. The other half of the cultures were placed on top of two LEDs (for each culture) operated at the same power, but covered with black tape so that no light would penetrate. The spatial arrangement of illuminated and non-illuminated cell culture flasks was randomized.

Light also affects the movement behavior of *E. gracilis* individuals through a process known as phototaxis, the directed movement of cells towards or away from light (Drescher et al. 2010; Giometto et al. 2015). Specifically, at low to intermediate light intensities, *E. gracilis* swims towards the light source at a time scale much shorter than the typical generation time. At very high light intensities, negative phototaxis can also be observed, and the plastic reaction of phototaxis can be induced very reliably (Giometto et al. 2015). The light intensity value used in our experiments is smaller than the light intensity value at which negative phototaxis occurs.

The front propagation experiment was performed in linear landscapes, which were channels drilled on a plexiglass sheet (5 mm wide, 3 mm deep and 1.9 m long, respectively, 300, 200 and 10^5 times the size of an individual, see Giometto et al. 2013), filled with filtered nutrient medium (fig. 2A). A gasket

avoided water spillage and a plexiglass lid was used to seal the system. The experimental replicates were kept in a climatized room at 22 °C for the whole duration of the experiment. Heterogeneous distributions of resources were generated via linear arrays of LEDs (fig. 2B) controlled via Arduino Uno boards. LEDs in the array were separated by a distance of $\Delta L = 3.12$ cm from each other and could be switched on or off individually. Switched-on LEDs emitted light with an intensity of $5.2 \text{ W}\cdot\text{m}^{-2}$ within the plexiglass channel, immediately above the LED. The linear landscapes were placed on top of the LED array at a distance of 4.5 mm. The light intensity profile generated by one LED was measured by placing a white paper sheet inside the plexiglass channel and by measuring the irradiance on the sheet with a digital camera operated in grayscale. The total radiant flux of the LED was measured via a calibrated photodiode. Light intensity profiles with the desired autocorrelation length were designed by imposing the probability λ of the LED number $i + 1$ in the LED array to be switched-on if the LED number i was switched-off, that is, $\mathbb{P}[\text{LED}(i + 1) = \text{ON} \mid \text{LED}(i) = \text{OFF}] = \lambda$. Such Markov Chain was imposed to be symmetric, that is, $\mathbb{P}[\text{LED}(i + 1) = \text{OFF} \mid \text{LED}(i) = \text{ON}] = \lambda$. Small and large values of λ generate resource distributions with long and small autocorrelation lengths (approximately equal to $\Delta L / (2\lambda)$), respectively. Because landscapes were of finite total length, the above procedure could generate by chance resource profiles with autocorrelation length different from the desired one and with a mean frequency of switched-on LEDs different from 1/2. Therefore, the set of resource profiles obtained with the above Markov Chain procedure was restricted to those with a mean frequency of switched-on LEDs equal to 1/2 and in a narrow window of autocorrelation length around the desired one. Therefore, all replicates had the same mean light intensity $\bar{I}(x) = L^{-1} \int_0^L I(x) dx$.

We compared two treatments in the experiment. Treatment 1 consisted of landscapes with identical small autocorrelation length ($c_L \simeq 2$ cm) but different switched-on LED sequences, generated via the Markov Chain procedure with $\lambda = 0.75$. Treatment 2 consisted of landscapes with identical large autocorrelation length ($c_L \simeq 6$ cm) but different switched-on LED sequences, generated via the Markov Chain procedure with $\lambda = 0.25$. The choice of the large autocorrelation length value in the experiment was limited by the total finite length of the experimental setup and was chosen to be less than 1/20 of the total setup length. We initially had six landscape replicates of each treatment, but lost one replicate of Treatment 1 due to leakage. All 11 landscapes had the same total number of switched-on LEDs and the experimental light intensity profiles are shown in fig. 3. The stated values of autocorrelation length are based on the first-order autocorrelation of the Markov Chain that generated the landscape. The first three LEDs in every landscape were switched-on to allow the local establishment of the inoculated *E. gracilis* population and to avoid differences between the two treatments in the initial establishment dynamics. Thus, the landscapes generated via the Markov Chain procedure described in the text started at the fourth LED. In Treatment 2 (large autocorrelation length), three landscapes were chosen so that the fourth LED was switched on and the other four were chosen so that the fourth LED was switched off. In other words, the realized Markov Chain started from its stationary distribution. The spatial arrangement of landscapes belonging to the two treatments on the experimental bench was randomized.

At the start of the experiment, we introduced an ensemble of *E. gracilis* individuals at one end of the linear landscapes. Following the inoculation, we measured for eight consecutive days the density of *E. gracilis* throughout all replicates by taking pictures with a stereomicroscope (model Olympus SZX16 with the digital camera Olympus DC72) and counting individuals via image analysis (Altermatt et al. 2015).

Statistical analysis

We used a mixed effect model to compare the speed of the propagating *E. gracilis* among the two different treatments. Thereby, the autocorrelation treatment was included as a fixed effect, while day and replicate were included as random effect. We repeated this analysis using different choices of threshold values used for determining the front position. The minimum and maximum threshold values employed in the statistical analysis were chosen such that no replicate displayed a retreating front between successive measurements (caused by noise in the density profiles). The test statistics are reported in table 1 for the density threshold value $\bar{\rho} = 60 \text{ cm}^{-1}$ and in table A1 for all values of $\bar{\rho}$ considered. We did not include the first timepoint in the analysis because it was measured immediately after the inoculation of *E. gracilis* in the landscape and thus was identical for all replicates. Because the propagating front reached the end of the landscape at day 4 in some replicates, the front propagation analysis was performed only with the data up to day 3 (included) to avoid spurious border effects due to the finite size of the system.

Model with directed movement towards resources

Equation (1) does not assume directed movement of individuals towards resources; such directed movement, however, occurs in our experiment and is likely to occur in nature (Andow et al. 1990; Fronhofer et al. 2013). Additionally, the experimental resource distributions (i.e., the light intensity profiles $I(x)$) were not simply sequences of illuminated and non-illuminated spatial patches with sharp edges, but, rather, smooth light intensity profiles alternating between well-lit and dark regions of the landscape according to the spatial arrangement outlined above. Because *E. gracilis* is capable to detect light intensity gradients and to move towards well-lit regions of the landscape, such directed movement may affect the invasion dynamics. To assess the net contribution of the directed movement of individuals towards resources, we incorporated in equation (1) the model for phototaxis derived in Giometto et al. (2015). The phototactic term was inferred from measurements of stationary density distributions of *E. gracilis* in the presence of light gradients and was shown to reproduce the accumulation dynamics of *E. gracilis* populations accurately in Giometto et al. (2015). The model equation reads:

$$\frac{\partial \rho}{\partial t} = \frac{\partial}{\partial x} \left[D \frac{\partial \rho}{\partial x} - \frac{d\phi}{dx}(I) \rho \right] + r(I) \rho \left[1 - \frac{\rho}{K} \right] + \sigma \sqrt{\rho} \eta, \quad (3)$$

where $\phi = a(I - I_c)/(I + I_r)$ is the phototactic potential describing *E. gracilis*' attraction towards (or against) light (Giometto et al. 2015). The parameters describing ϕ were estimated (Giometto et al. 2015) and were set equal to $a = 1.4 \cdot 10^{-8} \text{ m}^4 \cdot \text{W}^{-1} \cdot \text{s}^{-1}$, $I_r = 1.7 \text{ W} \cdot \text{m}^{-2}$ and $I_c = 28 \text{ W} \cdot \text{m}^{-2}$. We assumed that r follows Monod kinetics (the assumption is customary for phytoplankton, Diehl 2002), that is, $r(I) = r_1 I / (I + K_I)$, where K_I is the half-saturation constant. The model (equation 3) was integrated with parameters suitable to describe the experimental system, $r_1 = 6 \cdot 10^{-3} \text{ min}^{-1}$, $K_I = 1 \text{ W} \cdot \text{m}^{-2}$, $K = 300 \text{ cm}^{-1}$, $D = 0.08 \text{ cm}^2 \cdot \text{min}^{-1}$ (estimated in Giometto et al. 2015), various values of σ (fig. A8) and initial condition localized at the origin. See app. A for details on the numerical integration scheme adopted. The slowdown effect caused by the resource autocorrelation structure is also found with other choices of the growth rate dependence on the resource density. In fact, we found that results do not change qualitatively by assuming a linear dependence of r on I . We used equation (3) to simulate biological invasions in linear landscapes with resource distributions $I(x)$ exhibiting various autocorrelation lengths. To mimic the experimental setup (fig. 3), such landscapes were generated with the same Markov-chain procedure used

to design the experimental landscapes (see *Experiment* section), where the light intensity profile generated by a single LED (centered in $x = 0$) was assumed equal to the best fit of the equation $I(x) = c_0 / (c_1^2 + x^2)^2$ to the measured light intensity profile (see fig. S1 of Giometto et al. 2015). The total light intensity was kept constant for all landscapes. To further mimic the experiment, we set reflecting boundary conditions for the integration of equation (3) and simulations in which the population went extinct were excluded from the analysis. Therefore, the model equation (3) was specifically derived to reproduce as closely as possible the experimental system at hand. Landscapes used in the simulations were much longer (18 m) than those used in the experiment in order to avoid border effects. Such numerical settings allowed a clear identification of the invasion front and allowed simulating species spread in landscapes with very large autocorrelation length, which could not be investigated experimentally because of the finite size of the experimental setup.

Results

Our generalization of the Fisher-Kolmogorov equation (equations 1 and 2) includes demographic stochasticity and resource heterogeneity. Such resource heterogeneity affects the spread dynamics through the dependence of the growth rate r on the local amount of resources I (Methods). We found that the speed of invasion in the model equation (2) decreases with increasing resource autocorrelation length (fig. 1B). The mean front propagation speed, in heterogeneous landscapes where resource patch lengths are distributed exponentially with rate μ , depends on c_L and σ asymptotically (i.e., for large c_L and σ) as:

$$v = \frac{L}{\frac{\mu L}{2} \int_0^L dz \langle \tau \rangle(z, \sigma) \mu e^{-\mu z}} \simeq \frac{8c_L^2}{\int_0^\infty dz \langle \tau \rangle(z, \sigma) e^{-z/(2c_L)}}. \quad (4)$$

Figs. 1B and A2 show that equation (4) correctly predicts the speed of invasion at large values of c_L and σ . In heterogeneous landscapes with different spatial arrangements of favorable and unfavorable patches, if the percentage of space occupied by unfavorable patches is $f_0 \in (0, 1)$ and the distribution of such patches lengths is $p_0(z)$, with mean $\int dz z p_0(z) = 1/\mu$, the asymptotic invasion velocity can be approximated as:

$$v = \frac{1}{\mu f_0 \int_0^\infty dz \langle \tau \rangle(z, \sigma) p(z)}. \quad (5)$$

We show in the app. A that equation (5) correctly predicts the speed of invasion in landscapes with percentages of unfavorable habitat different from $f_0 = 1/2$ (fig. A5). Note that the speed of invasion according to equations (4,5) is a function of the autocorrelation length if the landscapes consist of favorable and unfavorable patches generated through the telegraph process outlined in the Methods section. In general, however, the speed of invasion is not a univocal function of the resource autocorrelation length (or of other characteristic length scales of the landscape), but it rather depends on the whole distribution of unfavorable patch lengths through equation (5). The slowdown effect is due to the fact that, in the presence of demographic stochasticity, long patches of unfavorable habitat act as obstacles for the spread of populations. The larger the extent of the unfavorable patch, the longer it takes for a population to cross it. The front propagation speed is also found to be a monotonically decreasing function of the amplitude of demographic stochasticity (fig. 1B). Accordingly, integrating the model without demographic stochasticity ($\sigma = 0$ in equation 2, gray dots in fig. 1B) leads to no discernible slowdown of the front in strongly autocorrelated versus weakly autocorrelated landscapes, even when imposing negative values of

the growth rate r in unfavorable patches where $I = 0$ (app. A). Such results demonstrate that the local extinctions caused by demographic stochasticity in unfavorable patches are responsible for the observed front slowdown.

Numerical integration of equation (2) shows that the variability of the front position increases for larger values of c_L and σ . Such increased variability is caused by two factors: i) two landscapes with identical resource autocorrelation lengths appear increasingly dissimilar for increasing values of the typical patch length $1/\mu$; ii) the variance of the distribution of waiting times (i.e., the times to cross an unfavorable patch of length z) increases (approximately) quadratically with the mean time $\langle\tau\rangle(z, \sigma)$ (fig. A3). These two observations can be used to approximate the fluctuations of the total time spent by the front to colonize a landscape of length L (fig. A4), as shown in the app. A.

The model (equations 1 and 2) assumes random local movement of individuals. Although such assumption may be appropriate to describe spread in homogeneous landscapes (Andow et al. 1990; Giometto et al. 2014), individuals might be able to exploit local information on the availability of resources to direct their movement towards more favorable regions (Andow et al. 1990; Fronhofer et al. 2013, 2015). We studied the effect of biased movement towards resources by including an advection term (towards regions endowed with more resources) in equation (1), leading to equation (3). The latter model predicts again that the front propagation speed decreases for increasing resource autocorrelation length, in accordance with the former model (equation 1). Integrating equation (3) with and without the advection term shows that the biased local movement towards resources causes an increased slowdown of the invasion front in strongly (compared to weakly) autocorrelated landscapes (fig. A8). In other words, the biased movement towards resources acts as a spring that keeps the population in favorable patches and works against the exploration of unfavorable ones. Excluding demographic stochasticity from the model equation (3) leads again to the elimination of the slowdown effect (inset of fig. A8).

We designed an experiment with *E. gracilis* to test the slowdown effect on the front propagation caused by the spatial resource autocorrelation length. We observed a steady front propagation across all landscapes with a mean front propagation speed of 54 ± 9 cm/d (mean \pm SE). The mean total number of individuals was 2420 ± 110 (mean \pm SE) at the start of the experiment (day 0), 15000 ± 800 (mean \pm SE) at the end of the front propagation phase (day 4) and 27000 ± 4500 (mean \pm SE) at the end of the experiment (day 8). Thus, the invasion process was a combination of active, directed movement of individuals as well as reproduction. We found a significantly slower front propagation in landscapes in which the resources were strongly spatially autocorrelated (mixed effect model $p = 0.027$, see also table 1). The result is robust to changes of the threshold value at which the front position is evaluated (table A1, figs. 4C and A10). The slowdown effect is visible in fig. 4C, which shows the mean front position across replicated invasions in the two treatments.

Discussion

Our experiments show that the slowdown effect predicted by the stochastic models equations (1), (2) and (3) is found in microcosm experimental systems, which can be used to bridge theoretical models and natural systems (Benton et al. 2007). In these experiments the demographic and movement traits of the study species were fixed and dictated by the species. The accompanying models additionally allowed to single out the individual role and the mutual interconnections of all processes included in the equations to the propagation dynamics in landscapes with different resource autocorrelation lengths.

Our theoretical and experimental investigation advances our current understanding of the spread of invading organisms in heterogeneous landscapes by addressing the joint effect of spatial environmental autocorrelation and demographic stochasticity on the spread dynamics. As arguably all natural landscapes are characterized by heterogeneous distributions of resources and all populations are subject to demographic stochasticity, our model incorporates two key elements hitherto often overlooked in the modeling of biological spread. A major result of our work is that demographic stochasticity is a key factor in the slowdown of front propagation in heterogeneous landscapes. Such finding highlights the importance of including demographic stochasticity in theoretical models because of the many facets through which it affects species spread (Giometto et al. 2014; Hallatschek and Korolev 2009). The implications of the above results challenge the standard approach as stochastic effects are neglected by deterministic, Fisher-Kolmogorov-like models. Because the slowdown effect is only observed when demographic stochasticity is included in the models, our theoretical investigation suggests that the stochastic birth-and-death dynamics are the main drivers of the observed reduction in propagation speed, rather than the movement behavior of individuals in heterogeneous landscapes that has received so far most attention in the literature (Morales and Ellner 2002; Van Dyck and Baguette 2005). Previous studies have investigated the minimum percentage of suitable habitat that allows invasions to spread (Dewhurst and Lutscher 2009; With 2002; With and Crist 1995), suggesting that invasions cannot propagate in landscapes with mean resource density below a critical threshold. Our work shows, complementarily, that the spatial arrangement of resources affects species spread even if the total amount of available resources is kept constant. Thus, it is not only the mean resource density that matters for the front propagation dynamics, because the autocorrelation structure of landscape heterogeneity alone also affects species spread. Our investigation extends previous works that addressed the effect of temporal environmental fluctuations on species spread (Ellner and Schreiber 2012; Méndez et al. 2011) by showing that the autocorrelation length of the resource distribution should be added to the environmental factors that can slow species spread, along with temporal fluctuations of vital rates (Ellner and Schreiber 2012; Neubert et al. 2000), geometrical heterogeneities of the substrate (Bertuzzo et al. 2007; Méndez et al. 2004; Méndez et al. 2003) and demographic stochasticity (Hallatschek and Korolev 2009).

Our finding that larger autocorrelation lengths reduce the spread rate of invading species is compatible with the results of Bergelson et al. (1994), who performed a field experiment with the invading weed *Senecio vulgaris* and found that the average spatial distance between two generations along linear transects increased when favorable patches were uniformly distributed in space (in the parlance of our work, the transect featured a small autocorrelation length), compared to transects with clumped patches (i.e., endowed with large autocorrelation length). Bailey et al. (2000) performed spread experiments with the fungal plant pathogen *Rhizoctonia solani*. Such work provides a complementing view to our investigation by evaluating the effect of the inter-distance between favorable patches on the spread and identifying experimentally the existence of a percolation threshold at a critical level of inter-patch distance. In the framework addressed here, the analog of such percolation threshold corresponds to an autocorrelation length much larger than the average distance traveled by the front during one generation. There exist considerable differences in the experimental setup and the study system between this investigation and those in Bergelson et al. (1994) and Bailey et al. (2000). Most importantly, biased active movement towards favorable patches was present in the experiment performed here and embedded in equation (3), while passive dispersal was implemented in Bergelson et al. (1994). Both Bailey et al. (2000) and Bergelson et al. (1994) differ from this study because the landscape and the distribution of resources herein

are continuous, whereas they adopted discrete spatial distributions of favorable patches. Although such discrete distributions might provide a good approximation to some fragmented landscapes, continuous heterogeneous distributions may be equally likely to occur in nature. Compared to previous experimental efforts, we provide a general theoretical framework to interpret the dynamical processes underlying the realized invasions. The theoretical investigation of equations (1), (2) and (3), in fact, allowed isolating the net effect of each process embedded therein. Furthermore, the theoretical approximation to the mean speed of invasion in the model (equation 2) derived here allows to quantitatively predict the dependence of such mean speed on the resource autocorrelation length c_L , the strength of demographic stochasticity σ and the other species traits.

Our results have important implications for species spread in natural environments, which are generally characterized by resources (seen as any field controlling vital rates, especially reproductive ones) being heterogeneously distributed. The typical autocorrelation length of the resource distribution can be inferred from environmental data (Turner 2005; Urban et al. 2008) and can be used as a concise indicator for the propagation success of a species of interest. Furthermore, the spatial availability of resources is often altered by human activities, reinforcing the fragmentation of landscapes. In fact, habitat fragmentation may decrease significantly the autocorrelation length of the landscape through the introduction of qualitatively different patches in the natural environment (Holyoak et al. 2005; With 2002). Our results give quantitative grounds to field observations on the effect of environmental heterogeneity on species spread. For instance, Lubina and Levin (1988) observed pauses in the spread of the California sea otter (*Enhydra lutris*) in the presence of habitat discontinuities. Such pauses and the corresponding piecewise-linear propagation of the front (see fig. 2 of Lubina and Levin 1988) are also found in our model (fig. A7), which enables to relate the mean spatial extent of habitat discontinuities to the average speed of invasion through equations (4) and (5). An alternation between phases of halt and spread was also found in the range expansion of the cane toad (*Chaunus marinus*) in Australia (fig. 2 of Urban et al. 2008). Urban et al. (2008) performed an in-depth analysis of the effect of environmental heterogeneity on the spread of the cane toad in the field and found a statistically significant effect of environmental heterogeneity and, most importantly, of the spatial autocorrelation of environmental variables on the realized patterns of invasion speed. They found such effect in nature in a realized (not replicable) invasion, and thus they could only correlate the realized spread dynamics and its reduction with the landscape autocorrelation. Here, we have given a mathematical framework and an experimental proof showing that the slowdown effect caused by the spatial autocorrelation structure of the landscape is not an artifact of the mathematical model.

Conclusion

In conclusion, our work demonstrates the need to account for the intrinsic stochasticity of population dynamics to broaden our understanding of ecological processes occurring in spatially extended natural landscapes, which typically display various degrees of heterogeneity. Further work should be dedicated to the modeling and experimentation of species spread in temporally-varying landscapes and, possibly, spatially-heterogeneous landscapes that fluctuate in time. Drawing from the literature on population dynamics in temporally-fluctuating environments, understanding the causal link between the autocorrelation structure of fluctuations and the dynamics of species spread is a promising direction for future research in this area.

Acknowledgments

We thank Enrico Bertuzzo, Francesco Carrara, Lorenzo Mari and Amos Maritan for many useful discussions. We gratefully acknowledge the support by Swiss Federal Institute of Aquatic Science and Technology (Eawag) discretionary funds and Swiss National Science Foundation Projects 200021_157174 and PP00P3_150698.

References

- Altermatt, F., E. A. Fronhofer, A. Garnier, A. Giometto, F. Hammes, J. Klecka, et al. 2015. Big answers from small worlds: a user's guide for protist microcosms as a model system in ecology and evolution. *Methods Ecol. Evol.* 6:218–231.
- Andow, D. A., P. M. Kareiva, S. A. Levin, and A. Okubo. 1990. Spread of invading organisms. *Landscape Ecol.* 4:177–188.
- Bailey, D. J., W. Otten, and C. A. Gilligan. 2000. Saprotrrophic invasion by the soil-borne fungal plant pathogen *Rhizoctonia solani* and percolation thresholds. *New Phytol.* 146:535–544.
- Benincà, E., V. Dakos, E. H. Van Nes, J. Huisman, and M. Scheffer. 2011. Resonance of plankton communities with temperature fluctuations. *Am. Nat.* 178:E85–E95.
- Benton, T. G., C. T. Lapsley, and A. P. Beckerman. 2001. Population synchrony and environmental variation: an experimental demonstration. *Ecol. Lett.* 4:236–243.
- Benton, T. G., M. Solan, J. M. Travis, and S. M. Sait. 2007. Microcosm experiments can inform global ecological problems. *Trends Ecol. Evol.* 22:516–521.
- Bergelson, J., J. A. Newman, and E. M. Floresroux. 1994. Rates of weed spread in spatially heterogeneous environments. *Ecology* 74:999–1011.
- Bertuzzo, E., A. Maritan, M. Gatto, I. Rodriguez-Iturbe, and A. Rinaldo. 2007. River networks and ecological corridors: Reactive transport on fractals, migration fronts, hydrochory. *Water Resour. Res.* 43:W04419.
- Bonachela, J., M. A. Muñoz, and S. A. Levin. 2012. Patchiness and demographic noise in three ecological examples. *J. Stat. Phys.* 148:723–739.
- Campos, D., J. Fort, and V. Méndez. 2006. Transport on fractal river networks: application to migration fronts. *Theor. Popul. Biol.* 69:88–93.
- Croze, O. A., G. P. Ferguson, M. E. Cates, and W. C. K. Poon. 2011. Migration of chemotactic bacteria in soft agar: role of gel concentration. *Biophysical journal* 101:525–534.
- Dewhurst, S., and F. Lutscher. 2009. Dispersal in heterogeneous habitats: thresholds, spatial scales, and approximate rates of spread. *Ecology* 90:1338–1345.
- Diehl, S. 2002. Phytoplankton, light, and nutrients in a gradient of mixing depths: theory. *Ecology* 83:386–398.
- Doering, C. R., K. V. Sargsyan, and P. Smereka. 2005. A numerical method for some stochastic differential equations with multiplicative noise. *Physics Letters A* 344:149–155.
- Dornic, I., H. Chaté, and M. A. Muñoz. 2005. Integration of Langevin equations with multiplicative noise and the viability of field theories for absorbing phase transitions. *Phys. Rev. Lett.* 94:100601.
- Drescher, K., R. E. Goldstein, and I. Tuval. 2010. Fidelity of adaptive phototaxis. *Proc. Natl. Acad. Sci. U.S.A.* 107:11171–11176.

- Duncan, A. B., A. Gonzalez, and O. Kaltz. 2013. Stochastic environmental fluctuations drive epidemiology in experimental host-parasite metapopulations. *Proc. R. Soc. London Ser. B* 280:20131747.
- Ellner, S. P., and S. J. Schreiber. 2012. Temporally variable dispersal and demography can accelerate the spread of invading species. *Theoretical Population Biology* 82:283–298.
- Fisher, R. A. 1937. The wave of advance of advantageous genes. *Ann. Hum. Genet.* 7:355–369.
- Fontaine, C., and A. Gonzalez. 2005. Population synchrony induced by resource fluctuations and dispersal in an aquatic microcosm. *Ecology* 86:1463–1471.
- Fox, J. W., D. A. Vasseur, S. Hausch, and J. Roberts. 2011. Phase locking, the Moran effect and distance decay of synchrony: experimental tests in a model system. *Ecol. Lett.* 14:163–168.
- Fronhofer, E. A., T. Hovestadt, and H. J. Poethke. 2013. From random walks to informed movement. *Oikos* 122:857–866.
- Fronhofer, E. A., J. Klecka, C. J. Melian, and F. Altermatt. 2015. Condition-dependent movement and dispersal in experimental metacommunities. *Ecol. Lett.* 18:954–963.
- García-Carreras, B., and D. C. Reuman. 2011. An empirical link between the spectral colour of climate and the spectral colour of field populations in the context of climate change. *J. Anim. Ecol.* 80:1042–1048.
- Giometto, A., F. Altermatt, F. Carrara, A. Maritan, and A. Rinaldo. 2013. Scaling body size fluctuations. *Proc. Natl. Acad. Sci. U.S.A.* 110:4646–4650.
- Giometto, A., F. Altermatt, A. Maritan, R. Stocker, and A. Rinaldo. 2015. Generalized receptor law governs phototaxis in the phytoplankton *Euglena gracilis*. *Proc. Natl. Acad. Sci. U.S.A.* 112:7045–7050.
- Giometto, A., A. Rinaldo, F. Carrara, and F. Altermatt. 2014. Emerging predictable features of replicated biological invasion fronts. *Proc. Natl. Acad. Sci. U.S.A.* 111:297–301.
- Gonzalez, A., and R. D. Holt. 2002. The inflationary effects of environmental fluctuations in source-sink systems. *Proc. Natl. Acad. Sci. U.S.A.* 99:14872–14877.
- Hallatschek, O., and K. Korolev. 2009. Fisher waves in the strong noise limit. *Phys. Rev. Lett.* 103:108103.
- Hastings, A., K. Cuddington, K. F. Davies, C. J. Dugaw, S. Elmendorf, A. Freestone, et al. 2005. The spatial spread of invasions: new developments in theory and evidence. *Ecol. Lett.* 8:91–101.
- Holyoak, M., M. A. Leibold, and R. D. Holt. 2005. *Metacommunities: Spatial Dynamics and Ecological Communities*. The University of Chicago Press, Chicago.
- Kinezaki, N., K. Kawasaki, F. Takasu, and N. Shigesada. 2003. Modeling biological invasions into periodically fragmented environments. *Theor. Popul. Biol.* 64:291–302.
- Kolmogorov, A. N., I. G. Petrovskii, and N. S. Piskunov. 1937. A study of the diffusion equation with increase in the amount of substance, and its application to a biological problem. *Moscow University Mathematics Mechanics Bulletin* 1:1–25.

- Korolev, K. S., J. B. Xavier, D. R. Nelson, and K. R. Foster. 2011. A quantitative test of population genetics using spatiogenetic patterns in bacterial colonies. *Am. Nat.* 178:538–552.
- Lubina, J. A., and S. A. Levin. 1988. The spread of a reinvading species: Range expansion in the California sea otter. *Am. Nat.* 131:526–543.
- Massie, T. M., G. Withoff, N. Kucklunder, U. Gaedke, and B. Blasius. 2015. Enhanced Moran effect by spatial variation in environmental autocorrelation. *Nat. Commun.* 6:5993.
- Melbourne, B. A., H. V. Cornell, K. F. Davies, C. J. Dugaw, S. Elmendorf, A. L. Freestone, et al. 2007. Invasion in a heterogeneous world: resistance, coexistence or hostile takeover? *Ecol. Lett.* 10:77–94.
- Méndez, V., D. Campos, and J. Fort. 2004. Dynamical features of reaction-diffusion fronts in fractals. *Phys. Rev. E* 69:016613.
- Méndez, V., S. Fedotov, and W. Horsthemke. 2010. *Reaction-Transport Systems*. Springer, Berlin.
- Méndez, V., J. Fort, H. Rotstein, and S. Fedotov. 2003. Speed of reaction-diffusion fronts in spatially heterogeneous media. *Phys. Rev. E* 68:041105.
- Méndez, V., I. Llopis, D. Campos, and W. Horsthemke. 2011. Effect of environmental fluctuations on invasion fronts. *J. Theor. Biol.* 281:31–38.
- Morales, J., and S. Ellner. 2002. Scaling up animal movements in heterogeneous landscapes: the importance of behavior. *Ecology* 83:2240–2247.
- Nelson, D. R. 2012. Biophysical dynamics in disorderly environments. *Annu. Rev. Biophys.* 41:371–402.
- Nelson, D. R., and N. M. Schnerb. 1998. Non-Hermitian localization and population biology. *Phys. Rev. E* 58:1383–1403.
- Neubert, M. G., M. Kot, and M. A. Lewis. 2000. Invasion speeds in fluctuating environments. *Proc. R. Soc. London Ser. B* 267:1603–1610.
- Pachepsky, E., and J. M. Levine. 2011. Density dependence slows invader spread in fragmented landscapes. *Am. Nat.* 177:18–28.
- Roy, M., R. D. Holt, and M. Barfield. 2005. Temporal autocorrelation can enhance the persistence and abundance of metapopulations comprised of coupled sinks. *Am. Nat.* 166:246–261.
- Seymour, M., and F. Altermatt. 2014. Active colonization dynamics and diversity patterns are influenced by dendritic network connectivity and species interactions. *Ecology and evolution* 4:1243–1254.
- Shigesada, N., K. Kawasaki, and T. Ei. 1986. Traveling periodic waves in heterogeneous environments. *Theor. Popul. Biol.* 30:143–160.
- Simpson, M. J., K. K. Treloar, B. J. Binder, P. Haridas, K. J. Manton, D. I. Leavesley, et al. 2013. Quantifying the roles of cell motility and cell proliferation in a circular barrier assay. *J. R. Soc. Interface* 10:20130007.
- Skellam, J. G. 1951. Random dispersal in theoretical populations. *Biometrika* 38:196–218.

- Turner, M. G. 2005. Landscape ecology: what is the state of the science? *Annu. Rev. Ecol. Evol. Syst.* 36:319–344.
- Urban, M. C., B. L. Phillips, D. K. Skelly, and R. Shine. 2008. A toad more traveled: the heterogeneous invasion dynamics of cane toads in Australia. *Am. Nat.* 171:E134–E148.
- Van Dyck, H., and M. Baguette. 2005. Dispersal behavior in fragmented landscapes: routine or special movements. *Basic and Appl. Ecol.* 6:535–545.
- Vasseur, D. A. 2007. Environmental colour intensifies the Moran effect when population dynamics are spatially heterogeneous. *Oikos* 116:1726–1736.
- Vasseur, D. A., and J. W. Fox. 2009. Phase-locking and environmental fluctuations generate synchrony in a predator-prey community. *Nature* 460:1007–1010.
- Williamson, J., and S. Harrison. 2002. Biotic and abiotic limits to the spread of exotic revegetation species. *Ecol. Appl.* 12:40–51.
- With, K. A. 2002. The landscape ecology of invasive spread. *Conserv. Biol.* 16:1192–1203.
- With, K. A., and T. O. Crist. 1995. Critical thresholds in species' responses to landscape structure. *Ecology* 76:2446–2459.

Tables

Table 1: Mixed-effect test statistics

	Value	Std. Error	df	<i>t</i> -value	<i>p</i> -value
Intercept	45.98	3.27	44	14.04	$p < 10^{-4}$
Autocorrelation length	−11.61	4.43	9	−2.62	0.0279

Mixed-effect test statistics testing the speed of front propagation, with the autocorrelation length treatment as single fixed effect and time/replicate as random effect. The treatment with small autocorrelation length had 5 replicates, the treatment with large autocorrelation length had 6 replicates. The front position was measured at the density threshold value $\bar{\rho} = 60 \text{ cm}^{-1}$.

Figures

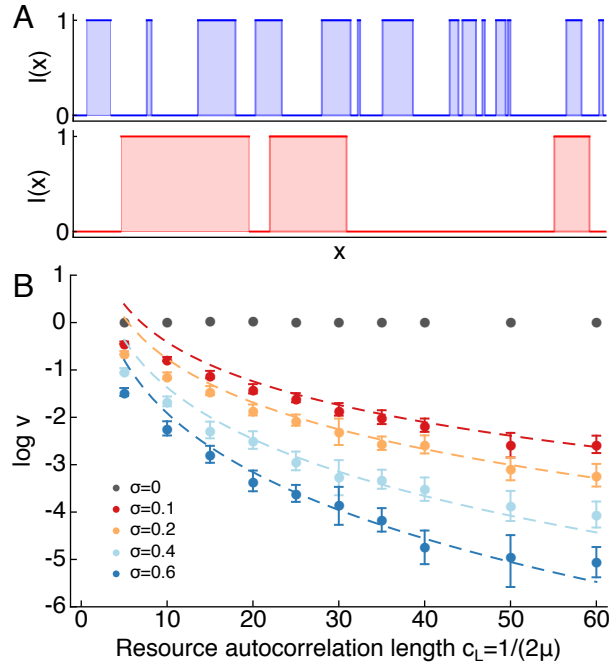


Figure 1: Mean front propagation in the model (dimensionless equation 2). (A) Examples of landscapes with different resource autocorrelation length c_L , generated via the telegraph process with rate μ (Methods). (B) The mean invasion speed computed in numerical integrations of the model (equation 2) decreases with increasing resource autocorrelation length c_L (log-linear plot) for $\sigma > 0$ and is a decreasing function of the amplitude of demographic stochasticity σ (different colors according to legend). With $\sigma = 0$ the dynamics is deterministic and the mean front propagation speed does not decrease with z (gray dots). Error bars display the 95% confidence interval for $\log v$, computed with $2 \cdot 10^3$ bootstrap samples. Error bars for $\sigma = 0$ are smaller than symbols. Dashed lines show the mean front propagation speed computed according to the theoretical approximation (equation 4).

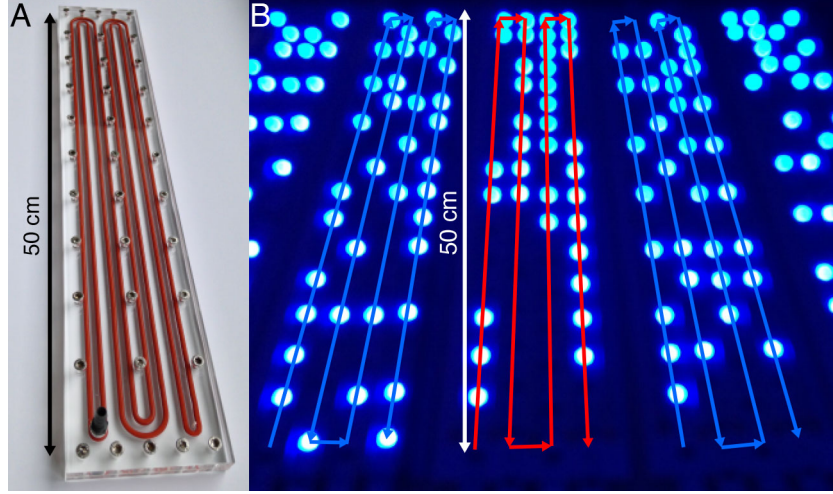


Figure 2: Experimental setup. (A) Linear landscapes used in the experiments were channels drilled on a plexiglass sheet. A gasket (orange rubber band) avoided water spillage. (B) Photograph of the LED strips used to control the distribution of resources for *E. gracilis*. The red and blue lines show the paths of landscapes with large and small resource autocorrelation length, respectively.

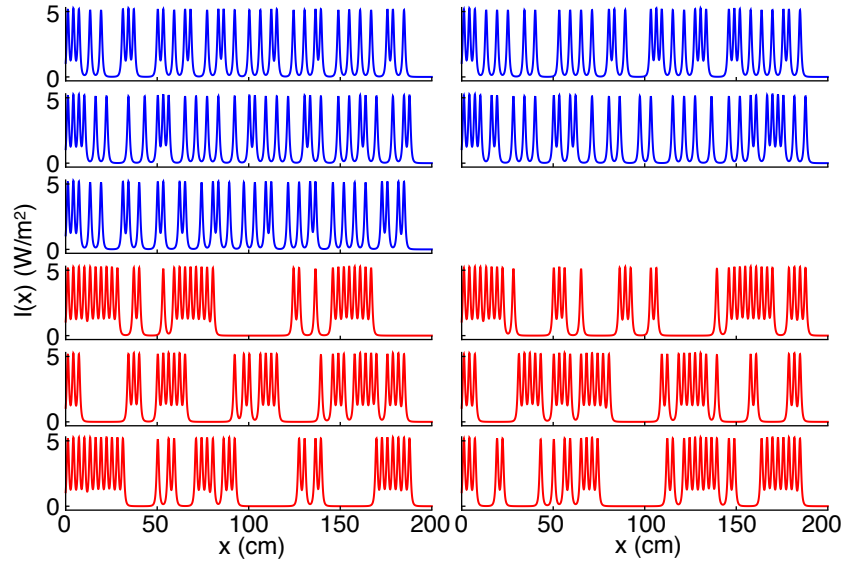


Figure 3: Light intensity profiles used in the experiment (Methods). One spread experiment was performed for each landscape. The total light intensity is the same for each landscape. Landscapes with the same color have identical small (blue) or large (red) autocorrelation length of the resource distribution $I(x)$, but different LED on-off sequences.

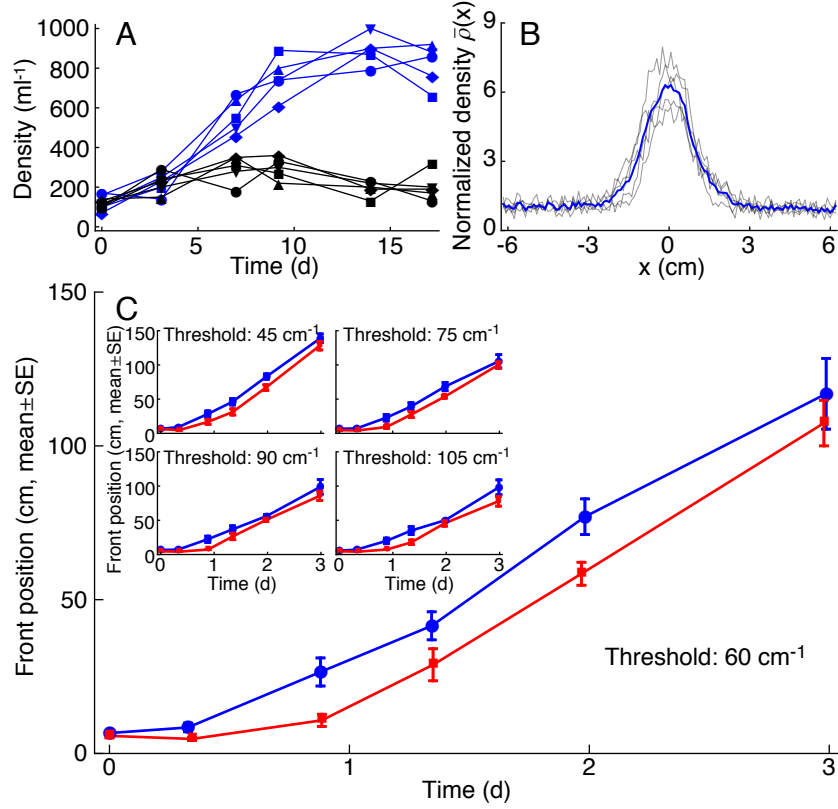


Figure 4: Experimental spread in autocorrelated landscapes. (A) Light was used as energy resource for *E. gracilis*. Replicated measured growth curves show that *E. gracilis* grows in the presence of light (blue symbols and lines) and does not grow in its absence (black symbols and lines). (B) Replicated measurements (gray lines) of *E. gracilis* density profiles (normalized by the value at the edge of the imaging window) in the presence of a LED at $x = 0$ cm show that *E. gracilis* populations accumulate around light sources through phototaxis. The blue line denotes the mean density profile across replicates (panel B is redrawn from Giometto et al. 2015). (C) Mean (\pm SE) position of the front, calculated among replicates with identical large (red) or small (blue) resource autocorrelation length at the threshold density value $\bar{\rho} = 60$ cm⁻¹. The inset shows mean front positions calculated at different threshold density values $\bar{\rho}$ as indicated. The slowdown effect is significant with all choices of $\bar{\rho}$, see Table A1.

Online Appendix A: Additional Methods and Results

A.1 Additional Methods

A suitable spatial discretization of equation (2) reads (Dornic et al. 2005; Giometto et al. 2014):

$$\frac{d\rho_i}{dt}(t) = \frac{1}{(\Delta x)^2} [\rho_{i+1}(t) + \rho_{i-1}(t) - 2\rho_i(t)] + r_i \rho_i(t) [1 - \rho_i(t)] + \frac{\sigma}{\sqrt{\Delta x}} \sqrt{\rho_i(t)} \eta_i(t), \quad (\text{A1})$$

where i identifies the lattice site, the term $\sqrt{\Delta x}$ ensures proper normalization in the continuum limit (Doering et al. 2005) and $r_i = \delta_{I_i,1}$ depends on the local value of the resource profile I (here, δ is the Kronecker's delta). The split-step method proposed in Dornic et al. (2005) was used to solve equation (A1). The spatial step in the numerical integration of equation (A1) was set to $\Delta x = 0.5$, while the temporal step was chosen equal to $\Delta t = 0.1$. The Courant-Friedrichs-Lewy condition for the diffusion equation $2\Delta t/\Delta x^2 < 1$ was thus satisfied and $\Delta t/\Delta x < 1$. The numerical integration of equation (A1) with $\sigma = 0$ was performed using the same numerical scheme, modified in the choice of ρ^* (we refer the reader to Dornic et al. 2005 for notation and symbols), which in the deterministic case is $\rho^* = \alpha/\beta (e^{\beta\Delta t} - 1) + \rho e^{\beta\Delta t}$. The deterministic equation was integrated with three choices of the growth rate r in unfavorable regions of the landscape (where $I = 0$), specifically $r = 0$, $r = -0.01$ and $r = -0.1$. None of these choices for r produced a slowdown of the front at large resource autocorrelation lengths, compared to small ones.

The spatial discretization of equation (3) reads:

$$\begin{aligned} \frac{d\rho_i}{dt}(t) = & \frac{D}{(\Delta x)^2} [\rho_{i+1}(t) + \rho_{i-1}(t) - 2\rho_i(t)] - \frac{1}{2\Delta x} [g_{i+1}\rho_{i+1}(t) - g_{i-1}\rho_{i-1}(t)] \\ & + r_i \rho_i(t) \left[1 - \frac{\rho_i(t)}{K} \right] + \frac{\sigma}{\sqrt{\Delta x}} \sqrt{\rho_i(t)} \eta_i(t), \end{aligned} \quad (\text{A2})$$

where $g = d\phi/dx[I(x)]$. The split-step method proposed in Dornic et al. (2005) was modified to solve equation (A2), which contains an advection term that might cause an artificial loss of mass if the step sizes are too coarse. Such issue does not occur with the step sizes $\Delta x = 0.6$ cm and $\Delta t = 0.5$ min⁻¹ chosen here. The Courant-Friedrichs-Lewy condition for the diffusion equation $2D\Delta t/\Delta x^2 < 1$ was satisfied and $\Delta t/\Delta x < 1$.

A.2 Additional Results

A.2.1 Mean front propagation speed in heterogeneous landscapes

Here we derive an approximation to the front propagation speed in the model equation (1), valid for large autocorrelation lengths and σ . We divide equation (1) by K and r_0 and rescale time as $t' = r_0 t$, which gives:

$$\frac{\partial \rho'(x, t')}{\partial t'} = \frac{D}{r_0} \frac{\partial^2 \rho'(x, t')}{\partial x^2} + \chi_I(x) \rho'(x, t') [1 - \rho'(x, t')] + \frac{\sigma'}{\sqrt{r_0}} \sqrt{\rho'(x, t')} \eta(x, t'), \quad (\text{A3})$$

where $\rho' = \rho/K$, $\sigma' = \sigma/\sqrt{K}$ and χ_I is the indicator function of the set of x for which $I(x) > 0$. We can further rescale space as $x' = \sqrt{\frac{D}{r_0}} x$ and rewrite equation (1) as:

$$\frac{\partial \rho'(x', t')}{\partial t'} = \frac{\partial^2 \rho'(x', t')}{\partial x'^2} + \chi_I(x') \rho'(x', t') [1 - \rho'(x', t')] + \sigma'' \sqrt{\rho'(x', t')} \eta(x', t'), \quad (\text{A4})$$

where $\sigma'' = \frac{\sigma'}{(rD)^{1/4}}$. In the following we will study the front propagation speed in the rescaled equation (2), where we drop primes for convenience; one can recover the original dimensions by multiplying t by r_0 and x by $\sqrt{r_0/D}$.

The rationale for our approximation of the mean front propagation speed is as follows. Let L be the finite length of a landscape and T the time taken by the population to reach the end of such landscape ($x = L$), starting from a localized initial condition at $x = 0$. For large values of autocorrelation length c_L and large enough σ , due to the local extinctions caused by demographic stochasticity, most of the time T is spent by the population trying to cross long patches of the landscape where $r = I = 0$. We can therefore approximate the mean front propagation speed for large c_L by computing the mean time that the front takes to cross an unfavorable patch of finite length z . Of course, such approximation is only valid when the waiting times dominate over the typical time scale of front propagation in favorable regions of the landscape. Therefore, the approximation can only hold for large enough values of the strength of demographic stochasticity σ .

A.2.1.1 Propagation past a patch of unfavorable landscape

We computed numerically the mean time $\langle \tau \rangle$ taken by the front to cross a region of landscape where $I = 0$, for different spatial extents of such region and different values of σ . We integrated numerically equation (2) in landscapes with resource profile $I(x) = \theta(x - z)$, where θ is the Heaviside step function. Such landscapes consist of a resource profile $I(x) = r(x) = 1$, except for $x \in (0, 1]$, that is a finite patch of spatial extent z at the left end of the landscape, where $I(x) = 0$. The initial condition was $\rho(x, 0) = 0$ for $x > 0$ and $\rho(0, 0) = k$, where k is the mean population density computed numerically by integrating equation (2) in a landscape of spatial extent $L = 100$ with growth rate profile $r(x) = 1$ for all $x \in [0, L]$. We fixed the Dirichlet boundary condition $\rho(0, t) = k$ and reflecting boundary conditions in $x = L$. We computed the mean time taken by the front to cross such unfavorable patch by measuring the first occurrence of $\rho(z) > 10^{-3}k$ in time. Fig. A1A shows the mean time $\langle \tau \rangle$ taken by the population to cross unfavorable patches of various extents z , computed for various values of σ . Such mean time $\langle \tau \rangle$ is a monotonically increasing function of both z and σ . To characterize the functional dependence of $\langle \tau \rangle(z, \sigma)$ on z and σ , we note that in the limit $\sigma = 0$ the dependence of $\langle \tau \rangle$ on z is that of the deterministic diffusion equation with boundary condition $\rho(0, t) = 1$, that is, $\tau(z, 0) = Cz^2$, where C is the solution of $\text{erfc}\left(\frac{1}{2\sqrt{C}}\right) = 10^{-3}$, where erfc is the complementary error function. We assume that $\langle \tau \rangle(z, \sigma)$ depends on z and σ through the functional form:

$$\langle \tau \rangle(z, \sigma) = Cz^2 F(z\sigma^b), \quad (\text{A5})$$

where $F(x)$ is a function that goes to the constant 1 for $x \rightarrow 0$. We can verify the validity of equation (A5) by plotting $z^{-2}\tau$ versus $z\sigma^b$ and varying b . Because we are able to find a value of $b = b^*$ for which data from the numerical integrations collapse onto one single curve (fig. A1B), the assumption on the functional form of $\langle \tau \rangle$ is verified. To further identify the functional dependence of $\langle \tau \rangle$ on z we plotted $\log[\log(z^{-2}\langle \tau \rangle) - \log C]$ vs $\log(z\sigma^b)$ and observed that simulation data aligned along a straight line. Therefore, our numerical analysis suggests that the functional dependence of τ on z and σ is given by:

$$\langle \tau \rangle(z, \sigma) = Cz^2 e^{d(z\sigma^b)^a}. \quad (\text{A6})$$

We estimated b by maximizing the R^2 (coefficient of determination) of the least-squares linear fit of $\log[\log(z^{-2}\langle \tau \rangle) - \log C]$ versus $\log(z\sigma^b)$. The slope and intercept of the linear fit with maximum R^2 gave

the estimate of a and d . Fig. A1 shows that equation (A6) reproduces the numerical data satisfactorily with the parameters $d = 0.74$, $a = 0.34$ and $b = 2.25$, identified as outlined above.

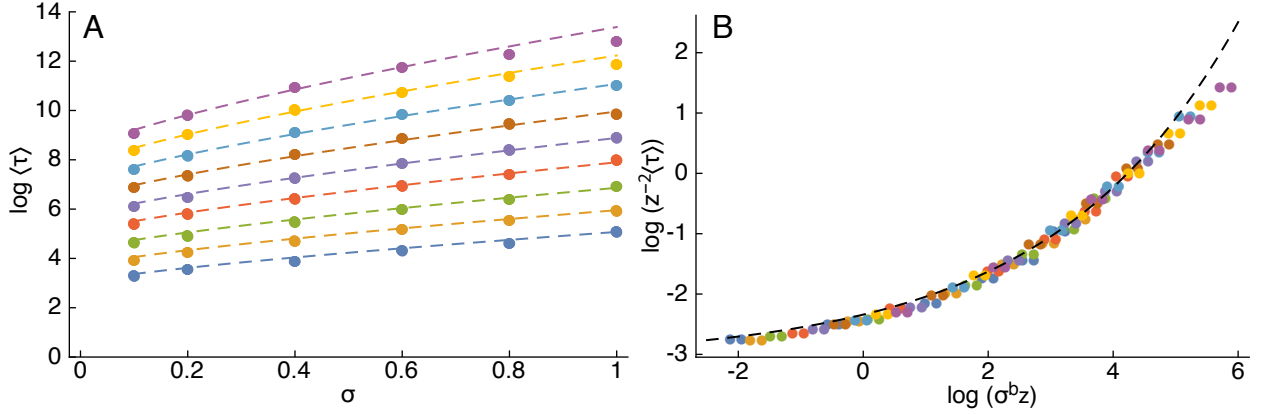


Figure A1: Mean time $\langle \tau \rangle$ taken by a diffusing population subject to demographic stochasticity to cross patches of length z , calculated for different values of z and σ across 192 integrations of equation (2). (A) τ is a monotonically increasing function of z and σ . Dots of identical color were computed with identical $z = 21, 29, 49, 57, 79, 111, 156$ and 218 , from bottom to top. Lines are computed via equation (A6), the color code identifies the value of z as for the dots. (B) Simulation data collapse onto the same curve when $z^{-2}\tau$ is plotted against $\sigma^b z$, proving the assumption made in equation (A5). Dots are color-coded as in panel (A), the dashed black line shows the function F computed according to equation (A6).

A.2.1.2 Approximation for the mean front propagation speed in heterogeneous landscapes

For large values of the autocorrelation length $c_L = 1/(2\mu)$ (μ is the rate of the telegraph process used to generate the heterogeneous landscapes, see Methods), most of the time taken by the front to propagate through a landscape of length L is spent trying to cross finite stretches of the landscape where $r = I = 0$. We can therefore approximate the front propagation speed as $v = L/T = L / \sum_{i=1}^N \langle \tau \rangle(z_i, \sigma)$ (black dots in fig. 4), where N is the number of unfavorable patches in $x \in [0, L]$ (of extent z_i) and $\langle \tau \rangle$ is the mean time taken to cross a patch of spatial extent z_i , estimated via equation (A6). In landscapes where unfavorable patches of length z occur with probability $\mu e^{-\mu z} dz$, one can approximate the mean front propagation speed for large autocorrelation length c_L as:

$$v = \frac{L}{\frac{\mu L}{2} \int_0^L dz \langle \tau \rangle(z, \sigma) \mu e^{-\mu z}} = \frac{c_L^2}{2 \int_0^L dz \langle \tau \rangle(z, \sigma) e^{-z/(2c_L)}}, \quad (\text{A7})$$

where $\langle \tau \rangle(z, \sigma)$ is given by equation (A6) and $\mu L/2$ at the denominator is the average number of unfavorable patches in the landscape. If L is comparable to c_L , one can substitute $\mu L/2$ with a more precise estimate, which is given in the next section. Fig. 4 shows that equation (A7) gives a good approximation to the front propagation velocities computed in the numerical integrations, for large values of c_L .

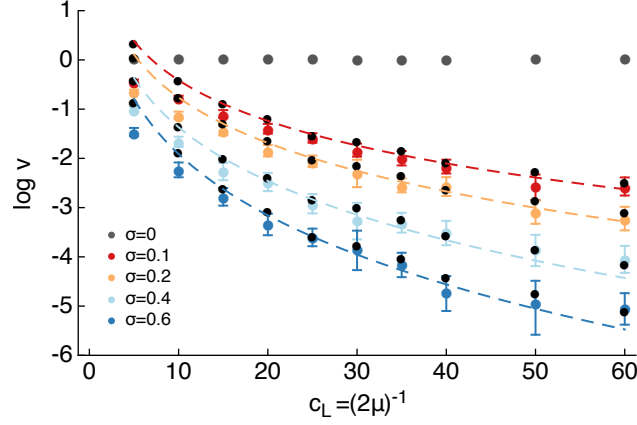


Figure A2: The mean front speed v decreases with increasing resource autocorrelation length $c_L = (2\mu)^{-1}$ (μ is the rate of the telegraph process used to generate the heterogeneous landscapes) and can be approximated by equation (A7) for large c_L (dashed lines). Colored data points highlight the mean speed v computed by numerically integrating equation (2) and by fitting the mean front position versus time to a straight line. Different colors refer to different values of σ according to the legend. Error bars display the 95% confidence interval for v , computed with $2 \cdot 10^3$ bootstrap samples. Error bars for $\sigma = 0$ are smaller than symbols. Dashed lines are the mean front speed computed according to equation (A7). Black dots are the approximation to the mean front speed computed as $v = L/T = L / \sum_{i \in Z} \langle \tau \rangle(z_i, \sigma)$, where Z is the set of unfavorable windows in the numerical landscapes. Dashed lines and black dots may differ because the numerical landscapes were finite, thus the distribution of unfavorable window lengths may differ slightly from the exponential pdf with typical length $1/\mu = 2c_L$.

A.2.1.3 Correction to the average number of patches if L is comparable to c_L

We provide here a correction to the term $\mu L/2$ at the denominator of equation (A7), which is relevant when $L \simeq c_L$. If the first patch at $x = 0$ is favorable (i.e., $r > 0$), the average number of unfavorable patches in a landscape of length L can be computed as follows. Let z_i be the rightmost coordinate of each patch in the landscape. The average number of unfavorable patches is equal to:

$$\langle N \rangle = \sum_{n=1}^{\infty} n \mathbb{P}[z_{2n} < L \cap z_{2n+1} \geq L] + \sum_{n=1}^{\infty} n \mathbb{P}[z_{2n-1} < 2 \cap z_{2n} \geq L].$$

Using properties of the exponential distribution of patch lengths one has:

$$\begin{aligned} & \mathbb{P}[z_{2n} < L \cap z_{2n+1} \geq L] \\ &= \mu^{2n+1} \int_0^L dz_1 e^{-\mu z_1} \int_{z_1}^L dz_2 e^{-\mu(z_2-z_1)} \dots \int_{z_{2n-1}}^L dz_{2n} e^{-\mu(z_{2n}-z_{2n-1})} \int_L^\infty dz_{2n+1} e^{-\mu(z_{2n+1}-z_{2n})} \\ &= \frac{e^{-\mu L}}{(2n)!} (\mu L)^{2n}, \\ & \mathbb{P}[z_{2n-1} < 2 \cap z_{2n} \geq L] \\ &= \mu^{2n} \int_0^L dz_1 e^{-\mu z_1} \int_{z_1}^L dz_2 e^{-\mu(z_2-z_1)} \dots \int_{z_{2n-2}}^L dz_{2n-1} e^{-\mu(z_{2n-1}-z_{2n-2})} \int_L^\infty dz_{2n} e^{-\mu(z_{2n}-z_{2n-1})} \\ &= \frac{e^{-\mu L}}{(2n-1)!} (\mu L)^{2n-1} \end{aligned}$$

and therefore:

$$\langle N \rangle = \sum_{n=1}^{\infty} n \left[\frac{e^{-\mu L}}{(2n)!} (\mu L)^{2n} + \frac{e^{-\mu L}}{(2n-1)!} (\mu L)^{2n-1} \right] = \frac{\mu L}{2} + \frac{e^{-\mu L}}{2} \sinh(\mu L),$$

where \sinh is the hyperbolic sine function. One can repeat the same analysis in the case where the first patch at $x = 0$ is unfavorable (i.e., $r = 0$). In this case one finds:

$$\langle N \rangle = \sum_{n=1}^{\infty} n \left[\frac{e^{-\mu L}}{(2n-2)!} (\mu L)^{2n-2} + \frac{e^{-\mu L}}{(2n-1)!} (\mu L)^{2n-1} \right] = \frac{\mu L}{2} + \frac{3}{4} + e^{-\mu L}.$$

Finally, if the first patch is favorable or unfavorable with equal probabilities, then:

$$\langle N \rangle = \frac{1}{2} \left[\frac{\mu L}{2} + \frac{e^{-\mu L}}{2} \sinh(\mu L) \right] + \frac{1}{2} \left[\frac{\mu L}{2} + \frac{3}{4} + e^{-\mu L} \right] = \frac{1}{2} + \frac{\mu L}{2}.$$

If $L \gg \frac{2}{\mu} = 4c_L$, the average number of unfavorable patches in a landscape of length L tends to $\frac{\mu L}{2}$.

A.2.2 Fluctuations of the invasion time

A.2.2.1 Fluctuations of the time taken to cross a patch of unfavorable landscape

In this section we study the fluctuations of the total invasion time in heterogeneous landscapes of finite size L . To this end, we first characterize the standard deviation σ_τ of the time τ taken by a diffusing population subject to demographic stochasticity to cross an unfavorable patch ($r = 0$) of spatial extent z . Inspection of the numerical results shows (fig. A3B) that $z^{-2}\sigma_\tau$ is a function of $z^{-2}\langle\tau\rangle(z, \sigma)$, that is:

$$\sigma_\tau(z, \sigma) = z^2 \mathbf{S} \left(z^{-2} \langle \tau \rangle (z, \sigma) \right), \quad (\text{A8})$$

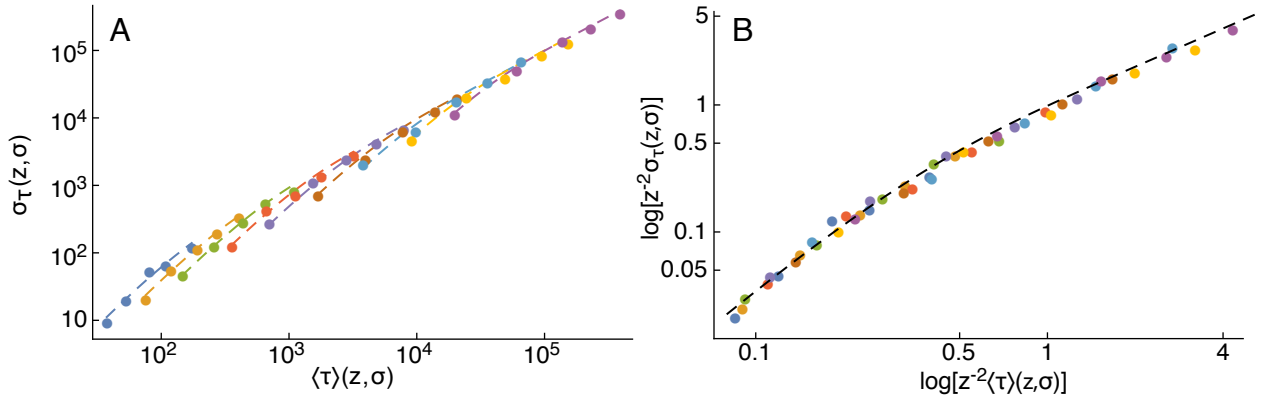


Figure A3: (A) Standard deviation σ_τ of the time taken by a diffusing population subject to demographic stochasticity to cross patches of length z , calculated for different values of z and σ across 96 integrations of equation (2) (double logarithmic plot). Different colors refer to different values of σ , from $\sigma = 0.1$ (blue dots at the bottom left corner) to $\sigma = 1.4$ (violet dots at the top right corner). Dashed lines are computed with equation (A9). (B) Simulation data collapse onto the same curve when $z^{-2}\sigma_\tau$ is plotted against $z^{-2}\langle\tau\rangle$, proving the validity of equation (A8). Dots are color-coded as in panel (A), the dashed black line shows the function \mathbf{S} computed according to equation (A9).

where $\mathbf{S}(x)$ is a function that goes to 0 for $x \rightarrow 0$. In fact, data from the numerical integrations of equation (2) in landscapes with resource profile $I(x) = \theta(x - z)$ (θ is the Heaviside step function, the same numerical data were used to derive equation A6) collapse on the same curve when $z^{-2}\sigma_\tau$ is plotted against $z^{-2}\langle\tau\rangle(z, \sigma)$ (fig. A3B). The functional form:

$$\sigma_\tau(z, \sigma) = \langle \tau \rangle(z, \sigma) \left[1 - e^{-kz^{-2}\langle \tau \rangle(z, \sigma)} \right] \quad (\text{A9})$$

is found to provide a good fit to the numerical data, with the best-fit estimate of the coefficient $k = 4.17$ (dashed lines in fig. A3).

A.2.2.2 Fluctuations of the total invasion time in heterogeneous landscapes

We can use equation (A9) to approximate the variance of the total invasion time T (i.e., the time after which the density $\rho(L, T)$ is larger than a threshold density value) in heterogeneous landscapes composed of favorable and unfavorable patches. In fact, the variance of the total invasion time in our simplified

model, where we neglect the time spent by the front in propagating through favorable patches, and further assuming that the times spent to cross each unfavorable patch are independent from each other, is given by:

$$\text{Var}[T] = \sum_{i=1}^N \sigma_{\tau}^2[\langle \tau \rangle(z_i, \sigma)], \quad (\text{A10})$$

where N is the number of unfavorable patches in $x \in [0, L]$ (patches of extent z_i) and σ_{τ} is given by equation (A9). We show in fig. A4 that equation (A10) gives a good estimate of the variance of the total invasion time in heterogeneous landscapes. Details are provided in the figure caption.

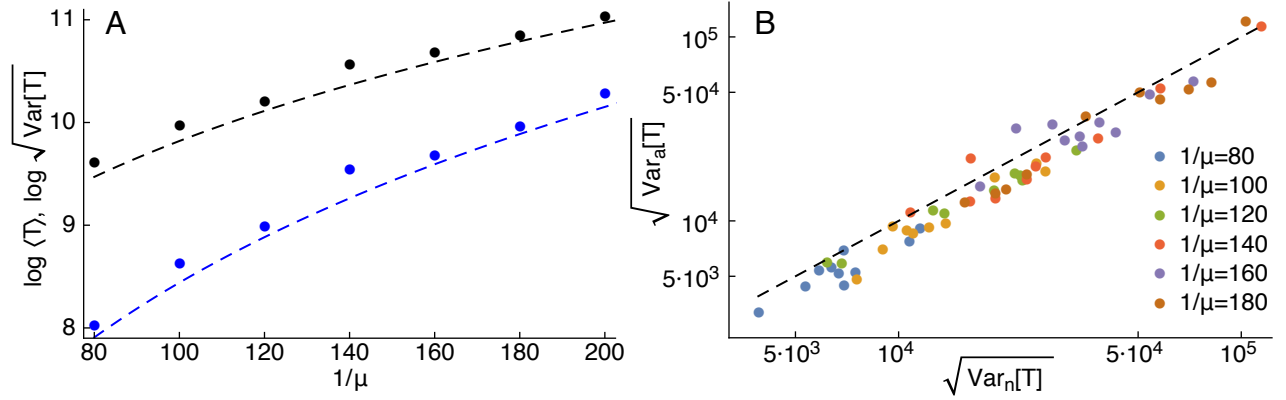


Figure A4: (A) Mean total time $\langle T \rangle$ (black dots) of invasion and its standard deviation (blue dots) in numerical integrations of equation (2) in square-wave landscapes of length $L = 1400$, that is, landscapes composed of alternated favorable and unfavorable patches of length $1/\mu$ (means and standard deviations were computed across 200 integrations for each value of $1/\mu$). The numerical estimates for $\langle T \rangle$ and $\sqrt{\text{Var}[T]}$ are well approximated by the approximations $\langle T \rangle = \frac{\mu L}{2} \tau(1/\mu, \sigma)$ (black dashed line) and by equation (A10) (blue dashed line). (B) Numerically computed standard deviations $\sqrt{\text{Var}_n[T]}$ (double logarithmic plot) of the total time T of invasion in numerical integrations of equation (2) in landscapes with exponentially-distributed favorable and unfavorable patches are well approximated by the theoretical approximation $\sqrt{\text{Var}_n[T]}$, computed according to equation (A10). Each dot represents one landscape of length $L = 2000$ and mean patch length $1/\mu$ according to the legend. Such landscapes were generated with the same procedure outlined in the Methods. To compute $\sqrt{\text{Var}_n[T]}$, we performed 96 numerical integrations for each landscape. The dashed black line is the 1:1 line. Numerical estimates and theoretical approximations are calculated with $\sigma = 0.4$ in both panels.

A.2.3 Front propagation at different mean resource densities

Other works (e.g., Dewhurst and Lutscher 2009) have studied the propagation of invasion fronts in landscapes with different average amounts of resources. One may wonder whether the slowdown effect caused by varying resource autocorrelation lengths of the resource distribution might also be found in landscapes endowed with mean percentages of suitable habitat different from $f_1 = f_0 = 1/2$. To show that such slowdown effect occurs also when the suitable and unsuitable habitats occur at different frequencies throughout the landscape, we have integrated equation (2) on landscapes endowed with various resource autocorrelation lengths and mean frequency of suitable (i.e., $r > 0$) and unsuitable (i.e., $r = 0$) habitat equal to $f_1 = 1/3$ and $f_0 = 2/3$, respectively. Such landscapes were generated as follows: we extracted the length of each favorable and unfavorable patch from exponential distributions with rate $\mu_1 = 3/(4c_L)$ and $\mu_0 = 3/(8c_L)$, respectively, so that the resource autocorrelation length was c_L and the frequencies of favorable/unfavorable habitat were as desired. Additionally, we have integrated equation (2) on the same landscapes switching each favorable patch of the landscape with an unfavorable one, so that favorable habitats occurred with frequency $f_1 = 2/3$ (and thus unfavorable habitats with frequency $f_0 = 1/3$). Fig. A5 shows that increasing the mean frequency of suitable habitat increases the invasion speed, but the slowdown effect caused by varying resource autocorrelation lengths is also present when favorable and unfavorable habitats occur at frequencies different from $1/2$. Furthermore, equation (5) can be used to approximate the mean speed of invasion for large c_L at values of f_0 different from $1/2$, as shown by the agreement between dashed lines and simulation data points in fig. A5.

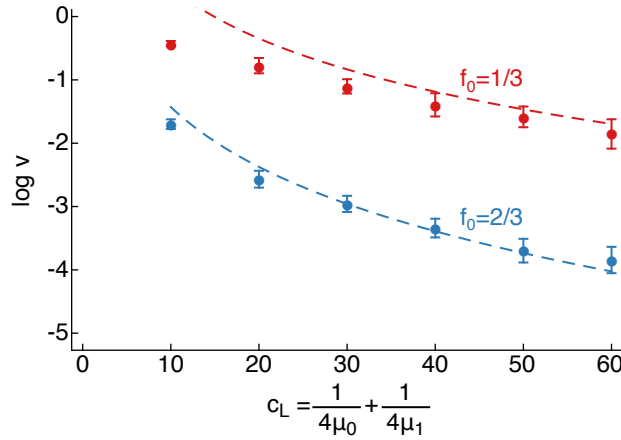


Figure A5: Mean front propagation speed in landscapes with favorable and unfavorable habitats occurring at frequencies different from $f_1 = f_0 = 1/2$. Red dots display the mean front speed in 96 replicated invasions in different landscapes with frequency of unsuitable habitat $f_0 = 1/3$. favorable patches lengths were distributed exponentially with rate $\mu_1 = 3/(8c_L)$ and unfavorable ones with rate $\mu_0 = 3/(4c_L)$. Blue dots display the mean front speed in 96 replicated invasions in different landscapes with frequency of unsuitable habitat $f_0 = 2/3$. Error bars display the 95% confidence interval for v , computed with $2 \cdot 10^3$ bootstrap samples. favorable patches lengths were distributed exponentially with rate $\mu_1 = 3/(4c_L)$ and unfavorable ones with rate $\mu_0 = 3/(8c_L)$. Dashed lines show mean front speeds approximated via equation (5) of the main text.

A.3 Additional Tables

Table A1: Mixed-effect test statistics for all choices of density threshold $\bar{\rho}$

Threshold $\bar{\rho}$		Value	Std. Error	df	t -value	p -value
45 cm^{-1}	Intercept	57.15	3.65	44	15.65	$p < 10^{-4}$
	Autocorrelation length	-11.31	4.94	9	-2.29	$p = 0.0480$
60 cm^{-1}	Intercept	45.98	3.27	44	14.04	$p < 10^{-4}$
	Autocorrelation length	-11.61	4.43	9	-2.62	$p = 0.0279$
75 cm^{-1}	Intercept	45.27	2.88	44	15.70	$p < 10^{-4}$
	Autocorrelation length	-9.65	3.90	9	-2.47	$p = 0.0355$
90 cm^{-1}	Intercept	36.65	2.84	44	12.91	$p < 10^{-4}$
	Autocorrelation length	-9.04	3.85	9	-2.35	$p = 0.0433$
105 cm^{-1}	Intercept	35.91	3.04	44	11.83	$p < 10^{-4}$
	Autocorrelation length	-10.79	4.11	9	-2.62	$p = 0.0276$

Mixed-effect test statistics testing the speed of front propagation, with the autocorrelation length treatment as single fixed effect and time/replicate as random effect. The treatment with small autocorrelation length had 5 replicates, the treatment with large autocorrelation length had 6 replicates. Different lines refer to different threshold values $\bar{\rho}$ at which the front position was measured.

A.4 Additional Figures

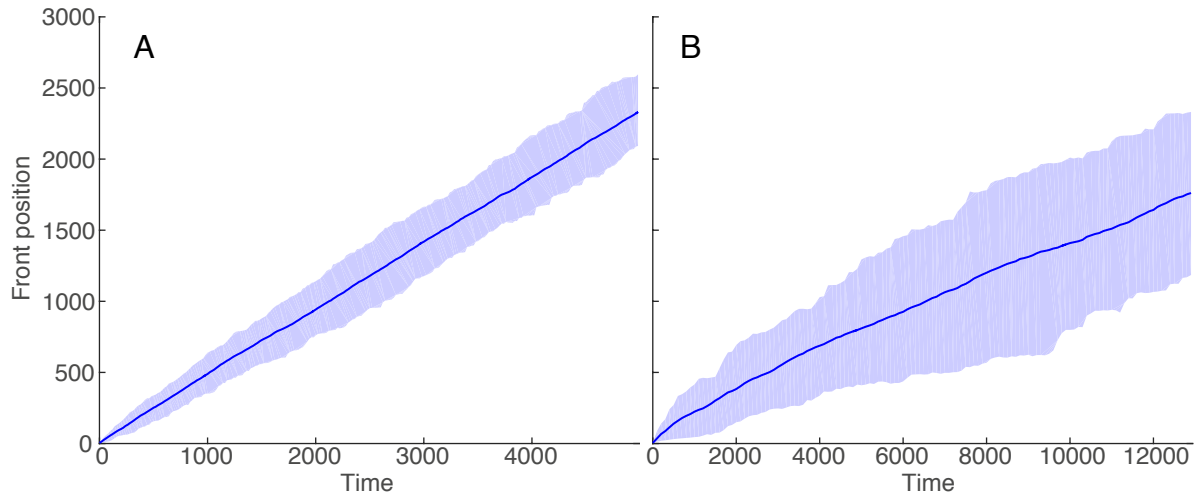


Figure A6: Mean position of the front (blue lines) and 68% confidence interval (shaded regions) in numerical integrations of the model equation (2) with $\sigma = 0.1$ and resource autocorrelation lengths $c_L = 5$ (A) and $c_L = 20$ (B).

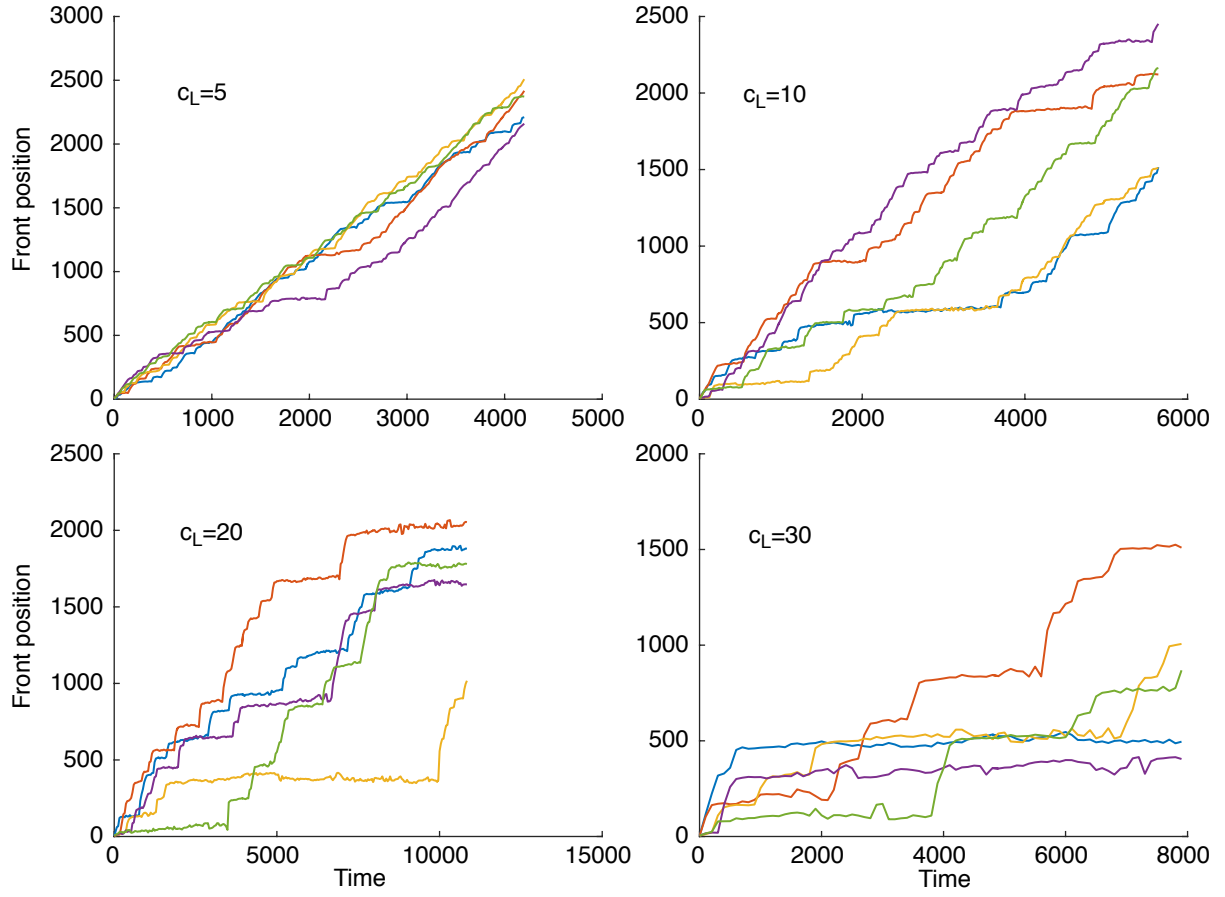


Figure A7: Examples of front propagation in numerical integrations of the model (equation 2) in landscapes with different resource autocorrelation lengths c_L and fixed amplitude of demographic stochasticity $\sigma = 0.2$.

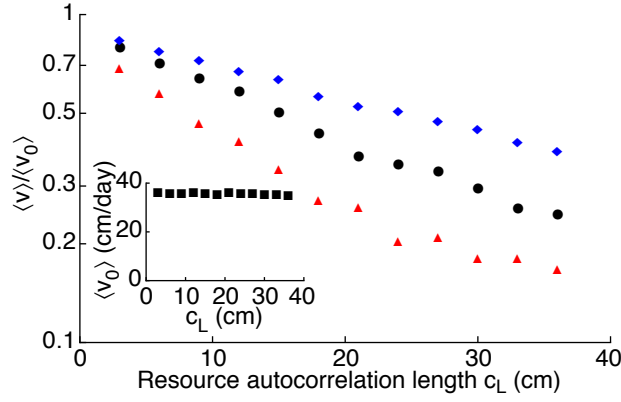


Figure A8: Front propagation computed in numerical integrations of the model equation (3) (with spatial discretization equation A2). The mean invasion speed decreases with increasing resource autocorrelation length $c_L = \Delta L / (2\lambda)$ (λ is the transition probability of the Markov Chain used to generate the heterogeneous landscapes and ΔL is the experimental distance between LEDs, see Methods) and is a decreasing function of the amplitude of demographic stochasticity σ (log-linear plot; black dots: $\sigma = 0.4 \text{ min}^{-1/2}$; red triangles: $\sigma = 0.7 \text{ min}^{-1/2}$). The mean speed of invasion is larger in the absence of directed movement towards resources (blue diamonds computed with $\sigma = 0.4 \text{ min}^{-1/2}$ and $\phi = 0$). Invasion speeds are reported here divided by the mean front speed $\langle v_0 \rangle$ at $\sigma = 0 \text{ min}^{-1/2}$, that is constant for different values of c_L (inset). The mean front speed for each value of c_L and σ was calculated by integrating equation (3) along 150 different landscapes with identical c_L and fitting the mean front position versus time in the asymptotic propagation regime.

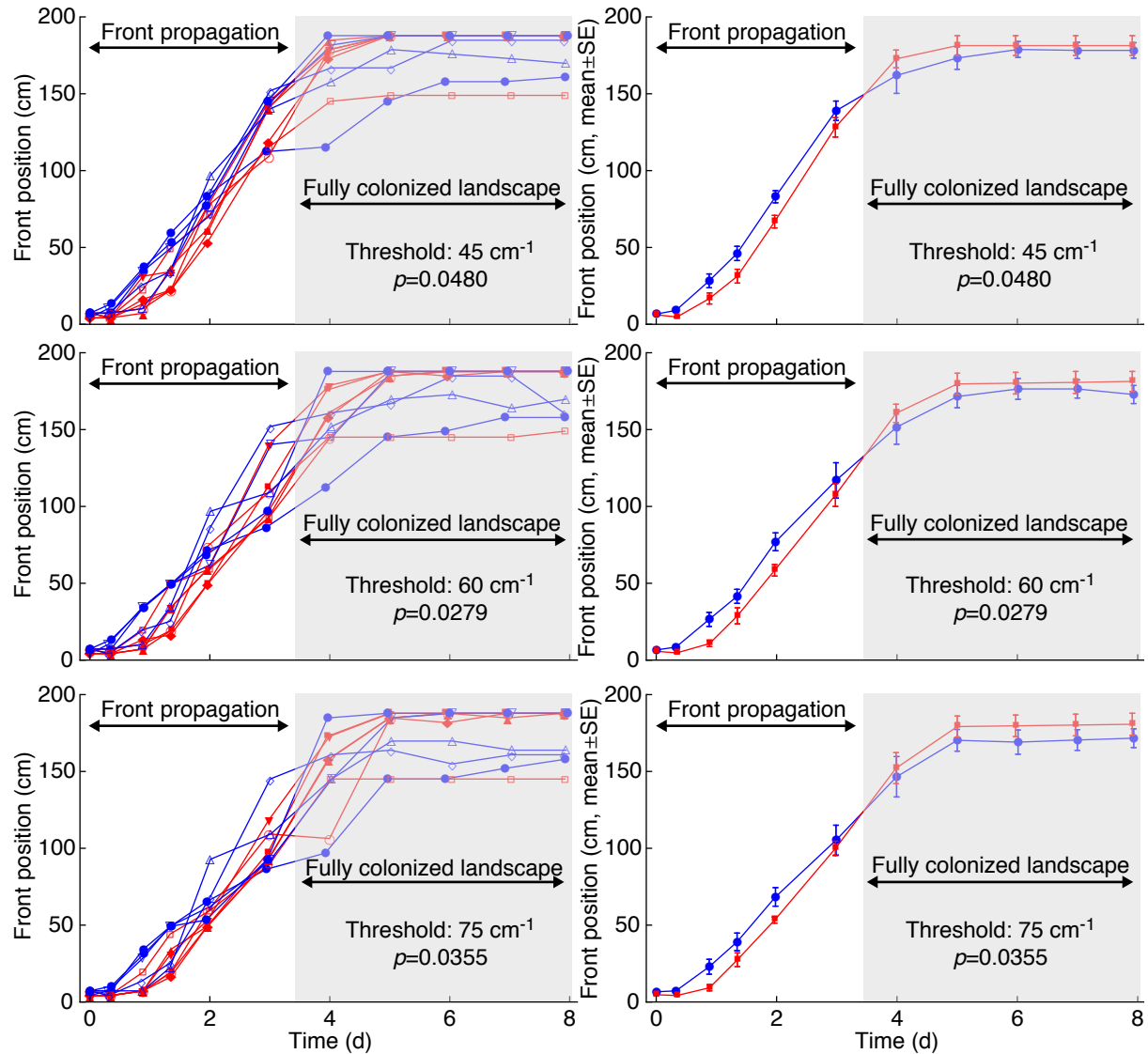


Figure A9: Experimental spread in autocorrelated landscapes. Left: position of the front in each experimental replicate, identified by different symbols. Red and blue lines and symbols refer to replicates with identical large (red) or small (blue) resource autocorrelation length. Right: mean (\pm SE) position of the front, calculated among replicates with identical large (red) or small (blue) resource autocorrelation length. Different rows refer to different threshold density values used to identify the position of the front. The gray shaded regions identify data points collected when at least one replicate had colonized the whole landscape. To avoid border effects, we excluded such points from the statistical analysis. In fact, at least one replicate with small autocorrelation length had reached the end of the landscape at time $t = 4$ d, and might have spread even further in a longer landscape. The reported p -values show that the autocorrelation treatment had a significant effect on the front propagation regardless of the choice of density threshold.

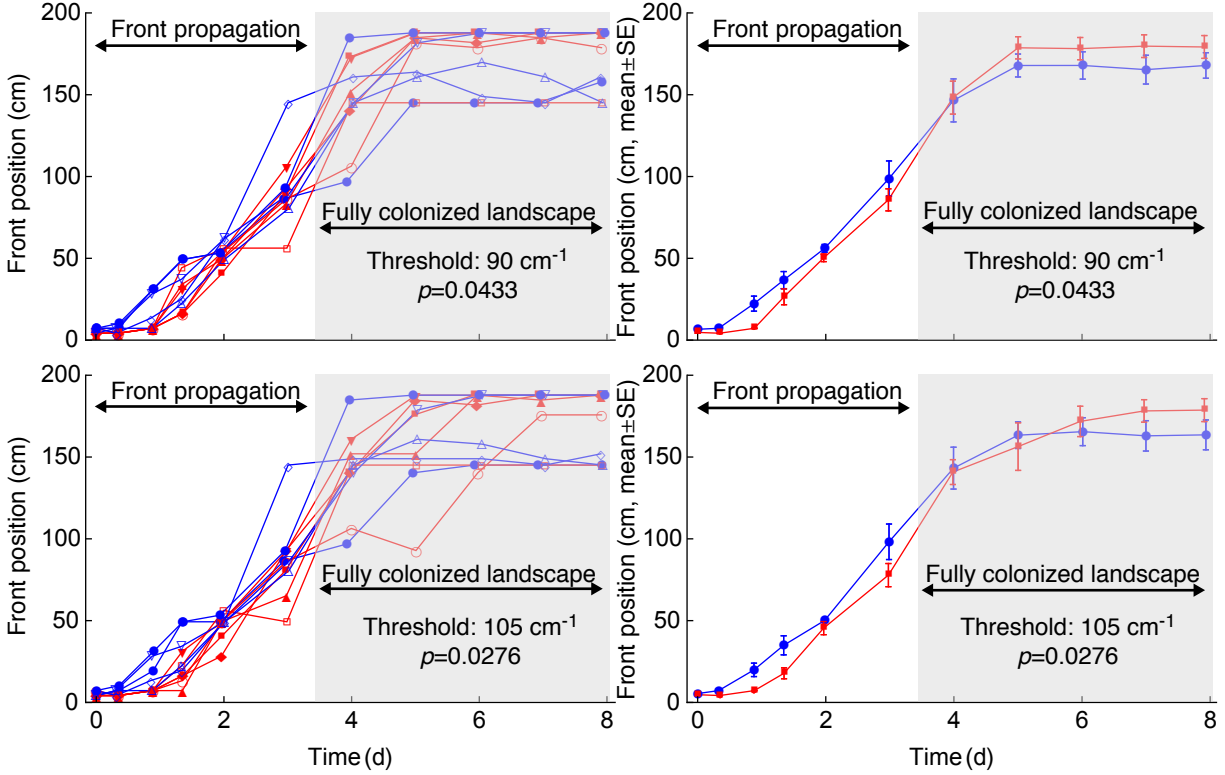


Figure A10: Experimental spread in autocorrelated landscapes. Left: position of the front in each experimental replicate, identified by different symbols. Red and blue lines and symbols refer to replicates with identical large (red) or small (blue) resource autocorrelation length. Right: mean (\pm SE) position of the front, calculated among replicates with identical large (red) or small (blue) resource autocorrelation length. Different rows refer to different threshold density values used to identify the position of the front. The gray shaded regions identify data points collected when at least one replicate had colonized the whole landscape. To avoid border effects, we excluded such points from the statistical analysis. In fact, at least one replicate with small autocorrelation length had reached the end of the landscape at time $t = 4$ d, and might have spread even further in a longer landscape. The reported p -values show that the autocorrelation treatment had a significant effect on the front propagation regardless of the choice of density threshold.